JOURNAL OF MORPHOLOGY 267:1099–1109 (2006)

Ontogeny of Form and Function: Locomotor Morphology and Drag in Zebrafish (*Danio rerio*)

Matthew J. McHenry[1]* and George V. Lauder[2]

[1]*Department of Ecology & Evolutionary Biology, University of California, Irvine, California 92697*
[2]*Department of Organismic and Evolutionary Biology, Harvard University, Cambridge, Massachusetts 02138*

ABSTRACT Many fish species transform in body shape during growth, but it remains unclear how this influences the mechanics of locomotion. Therefore, the present study focused on understanding how drag generation during coasting is affected by ontogenetic changes in the morphology of zebrafish (*Danio rerio*). The shapes of the body and fins were measured from photographs of fish ranging in size from small larvae to mature adults and these morphometrics were compared to drag coefficients calculated from high-speed video recordings of routine swimming. We found that the viscous drag coefficient of larval and juvenile fish increased by more than an order of magnitude during growth and the inertial drag coefficient decreased at a comparable rate in adults. These hydrodynamic changes occurred as zebrafish disproportionately increased the span of their fins and their body changed shape from elongated to streamlined, as reflected by the logistic growth of a newly defined streamlining index, S_L. These results suggest that morphological changes incur a performance cost by generating greater drag when larvae and juveniles operate in the viscous regime, but later provide a performance benefit by reducing pressure drag in the inertial regime of the adult stage. J. Morphol. 267: 1099–1109, 2006.

KEY WORDS: gliding; locomotion; swimming; fish; scaling; allometry; isometry

The mechanics of locomotion may transform dramatically over the growth of an aquatic animal due to changes in morphology and size-dependent hydrodynamics. Both factors figure prominently in the numerous species of fish that grow from a few millimeters to a few centimeters in length. Although zoologists have long appreciated the dramatic patterns of morphological change in these animals (e.g., Thompson, 1917), it remains unclear how growth affects the hydrodynamics of locomotion. Therefore, a prior study focused on understanding how hydrodynamic regimes scale with body size in zebrafish (*Danio rerio*: McHenry and Lauder, 2005) and the present study examined how changes in body shape affect drag generation in the same species.

Scaling of Drag

Inertial force plays an increasingly dominant role in the hydrodynamics of locomotion as a fish grows larger. The Reynolds number ($Re = \rho UL/\mu$, where U is flow speed, L is body length, and ρ and μ are, respectively, the density and dynamic viscosity of water; Lamb, 1945) normalizes the magnitude of this force relative to viscous force and thereby provides a nondimensional index of hydrodynamic scale. Therefore, measurements of Re indicate the relative contribution of inertial and viscous forces to the total force acting on a body. In a coasting fish, drag is primarily generated by viscous force at $Re <$ 300 and inertial force at $Re >$ 1,000 (McHenry and Lauder, 2005). In the viscous regime, drag may be normalized by the size and speed of the animal to yield the viscous drag coefficient ($C_{visc} = D/UL\mu$, where D is drag). The inertial drag coefficient ($C_{inert} = 2D / U^2S\rho$) provides a similar nondimensional measure of drag for the inertial regime (Lamb, 1945; Batchelor, 1967; Webb and Weihs, 1986; Osse and Drost, 1989; McHenry et al., 2003). These drag coefficients express the propensity of an animal's shape to generate drag within the appropriate regime, irrespective of body size or speed. Therefore, the present study used in vivo measurements of drag coefficients (Bilo and Nachtigall, 1980; McHenry and Lauder, 2005) to determine how shape change affects drag production over the course of growth.

Growth of Locomotor Morphology

Although many fishes grow from an elongated larval body to a streamlined adult, interspecific differences in morphology have confounded attempts to encapsulate this pattern with measurements of linear dimensions. For example, the trunk and caudal regions of both salmon (*Oncorhynchus tshawytscha*;

Contract grant sponsor: National Science Foundation (NSF) Postdoctoral Research Fellowship; Contract grant numbers: NSF IOB0509740 (to M.J.M.); IBN0316675 (to G.V.L.).

*Correspondence to: M.J. McHenry, 321 Steinhaus Hall, University of California, Irvine, CA 92697. E-mail: mmchenry@uci.edu

Published online 2 June 2006 in
Wiley InterScience (www.interscience.wiley.com)
DOI: 10.1002/jmor.10462

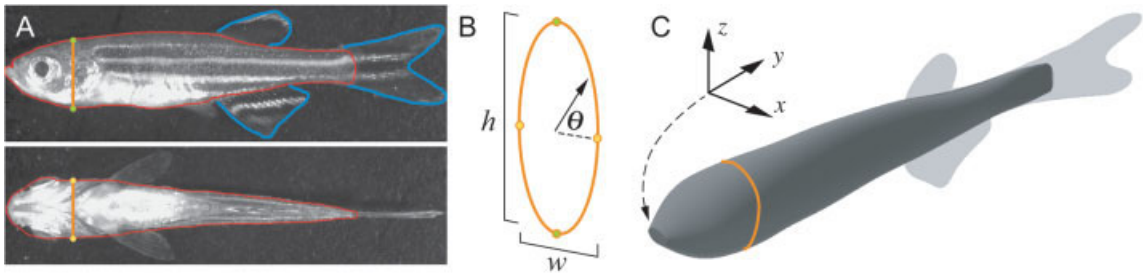

Fig. 1. Three-dimensional reconstruction of body shape from photographs. **A,B:** Reconstructions assumed an elliptical transverse shape, such as the one highlighted (orange lines) with dimensions based on measurements of the width (w, yellow points) and height (h, green points) of the body. **A:** Outlines of the body (red line) and median fins (blue line) were found from photographs of the lateral (top) and ventral (bottom) views. **B:** Measurements of the height and width of these outlines were used to reconstruct cross-sections of the body, which were defined with respect to their radial position (Θ) on the transverse plane. **C:** The body was reconstructed from a series of these transverse sections along its length in a right-handed xyz coordinate system with its origin anterior to the rostrum.

Hale, 1996) and pike (*Esox lucius*; Fuiman, 1982) become less elongated and more streamlined during growth. However, the fineness ratio (body length divided by its maximum height) decreases in pike and increases in salmon because salmon digest a relatively large yolk during the larval stage. Beyond providing an incomplete description of form, the fineness ratio is difficult to interpret functionally because it does not directly relate to a mechanical parameter, such as a drag coefficient.

Hydrodynamic theory provides a basis for interpreting how growth affects fish locomotion. As some species adopt a more streamlined shape, they move with greater intermittency and apparent maneuverability. It has been observed that these changes correlate with increases in size and speed that permit operating at $Re > 20$ (Webb and Weihs, 1986; Fuiman and Webb, 1988; Osse and van den Boogaart, 2000; Muller and van Leeuwen, 2004). Under the assumption that locomotor hydrodynamics become inertia-dominated at the $Re > 20$, it has been argued that streamlining serves as a drag-reducing adaptation to the hydrodynamics of routine swimming. According to this argument, changes in locomotor morphology match the immediate demands of the size-dependent hydrodynamics at each stage of growth. However, the hydrodynamic scaling assumed by these interpretations (based largely on the hydrodynamics of a sphere: Hoerner, 1965) was challenged by recent experimental evidence suggesting that larval fish are viscous-dominated up to $Re \approx 300$ (Fuiman and Batty, 1997; McHenry and Lauder, 2005). These findings raise the possibility that observed morphological and behavioral change precedes any dramatic shift in the hydrodynamics of routine swimming. In such conditions, the scale-dependency of hydrodynamics delays the functional benefits to streamlining and intermittent swimming until the fish are large enough to operate outside of the viscous regime.

In order to examine the immediate or delayed consequences of morphological growth, we related changes in morphology to the drag coefficients during coasting in zebrafish. This approach focused on addressing three specific questions. 1) How does the body change shape during growth? We measured linear dimensions and reconstructed the 3D shape of the bodies of fish from photographs to calculate surface area and a streamlining index. 2) How do the size and posture of the fins change during growth? The morphometrics and kinematics of the fins during coasting were compared across growth stages. 3) How do morphological changes affect drag coefficient? We measured the drag coefficients of coasting fish in vivo and compared how they changed with morphology and kinematics.

MATERIALS AND METHODS

Measurements were made using wildtype zebrafish, *Danio rerio* (Hamilton-Buchanan 1822), ranging in size from small larvae (~5 days postfertilization) to adults (>90 days postfertilization), with each fish categorized by stage of growth based on body length. Fish were considered small larvae if $L < 5.4$ mm (where L is body length), large larvae if 5.4 mm $< L <$ 8.9 mm, juveniles if 8.9 mm $< L <$ 18.0 mm, and adults if $L > 18.0$ mm (Schilling, 2002). All fish were maintained according to standard protocols (Westerfield, 1995) on a 14/10 h light/dark cycle at 26°C. Fish were euthanized by an overdose of MS-222 (Argent Laboratories, Redmond, WA) following kinematic experiments and prior to morphometric measurements. The present study was conducted in parallel with a previously reported project (McHenry and Lauder, 2005) that used some of the same subjects.

Body and Fin Morphometrics

The shape of the body and fins were measured from digital photographs of dead fish photographed from dorsal and lateral views. We used a digital camera (2048 × 1536 pixels in 8-bit grayscale, Nikon Coolpix 995) mounted onto a stereomicroscope at a magnification where the body length spanned approximately three-quarters of the camera frame. Silhouettes describing the shape of the body and fins were traced from these photographs (Fig. 1A) using Photoshop (v. 6.0, Adobe Systems, San Jose, CA) and converted to a binary image. The area and coordinates describing the peripheral shape of silhouettes were found using a custom program in Matlab (v. 6.5 with Image Processing Toolbox 4.0, MathWorks, Natick, MA) that required user input to specify coordinates for the rostrum, body midline, posterior margin of the caudal fin, dorsal and ventral margins of each median fin, and proximal and distal ends of the pectoral fins by visual landmarks.

Measurements of the median fins were made from the photographs of the lateral view, but the pectoral fins were photographed and measured from such an angle that the camera was perpendicular to a single fin (i.e., the view with maximum fin area). The span of the caudal fin was taken as the distance between its dorsal and ventral margins. The span of the dorsal and anal fins was considered the sum of distances between the dorsal and ventral margins of both fins and therefore excluded the height of the body. Similarly, the width of the body was excluded from measurements of the span of the pectoral fins, which was calculated as twice the distance between proximal and distal ends of a single fin.

The exponential growth in linear dimensions, body mass, and wetted surface area of the body and fins were evaluated by base-10 log-transformation and regression analysis. The exponential growth of these dependent parameters, y, were described by a scaling constant, a, and scaling factor, f, of an exponential function of body length ($y = a\,L^f$). Log-transformation of the independent and dependent variables in these exponential relationships yielded the equation for a line ($\mathrm{Log}_{10}\,y = f\,\mathrm{Log}_{10}\,L + \mathrm{Log}_{10}a$; Huxley, 1932). The scaling factor found from this curve fitting was statistically compared to an isometric prediction (f_o) using a reduced major axis regression analysis with Matlab (Sokal and Rohlf, 1995). This form of Type II regression analysis was appropriate in this case because the dependent variables could not be assumed to have the same scale or dimensions as body length measurements (Rayner, 1985). We considered growth to be allometric in cases where the isometric prediction ($f_o = 1$ for linear measurements, $f_o = 2$ for area, $f_o = 3$ for mass or volume) fell outside of the lower, f_{low}, and upper, f_{up}, 95% confidence intervals for the scaling factor (Rayner, 1985; McHenry and Jed, 2003).

The 3D shape of the body of a fish was reconstructed from measurements of its peripheral shape from dorsal and lateral views using a custom program in Matlab. This program first interpolated between coordinates of silhouettes of the body's periphery to find the height (h) and width (w) of the body at 200 equally spaced positions along the midline (Fig. 1A,B). The shape of the body in the transverse plane was calculated from these measurements by approximating its shape as an ellipse (Fig. 1B). This reconstruction of the body was performed in a right-handed xyz coordinate system with its origin at the anterior of the rostrum, its y-axis directed posteriorly and its z-axis directed dorsally (Fig. 1C). The transverse ellipses of the body provided x- and z-coordinates describing the shape of the body at each y-position:

$$x_{per} = \frac{w}{2}\,\mathrm{Cos}(\theta), \tag{1}$$

$$z_{per} = \frac{h}{2}\,\mathrm{Sin}(\theta) + z_{cen}, \tag{2}$$

where x_{per} and z_{per} are, respectively, the peripheral coordinates of the body's surface along the x- and z-axes, z_{cen} is the position of the center of the transverse section in the z direction, and Θ is the radial position of the periphery (100 equally spaced points over $0 \le \Theta \le 2\pi$; Fig. 1B). The surface of the body was defined by polygons connecting the coordinates of neighboring ellipses at the same radial position. Increasing the resolution beyond 200 midline positions and 100 radial positions ceased to influence morphometric measurements.

This volumetric description of the body allowed us to calculate a series of mechanically relevant morphometric parameters. We calculated the wetted surface area as the sum of area for all polygons describing the body's peripheral shape (within Matlab). Measurements of body mass in small larvae were confounded by adherent water or rapid desiccation and the limited sensitivity of our analytical balance (0.1 mg, Mettler AE50). Therefore, we calculated the mass of these fish as the product of the density of water and the integrated volume enclosed by the peripheral shape of the body.

In order to quantify the degree to which a body is streamlined, we compared its volume distribution to a body having the profile of a streamlined shape. Streamlined shapes were drawn from the family of foils classified by the U.S. National Advisory Committee for Aeronautics (NACA). The shape of the NACA family of 0000-series foils without camber may be described by its height, h_{NACA}, as a function of y in the following equation (Ladson et al., 1996):

$$h_{NACA}(y) = \frac{h_{max}}{2}\left(0.2969\left(\frac{y}{L}\right)^{1/2} - 0.1260\left(\frac{y}{L}\right) - 0.3516\left(\frac{y}{L}\right)^{2} + 0.2843\left(\frac{y}{L}\right)^{3} - 0.1015\left(\frac{y}{L}\right)^{4}\right) \tag{3}$$

where h_{max} is the height equal to the maximum height measured along the midline of the fish's body. The same equation was used to calculate the width, $w_{NACA}(y)$, of the streamlined body using the maximum width, w_{max}, of the fish's body and the transverse shape of these bodies were also assumed to be elliptical.

The distributions of volume for fish and NACA-streamlined bodies were compared by finding the ratio of their moments of inertia. The moment of inertia is calculated by dividing a body into numerous small volumes and then integrating the product of volumes by their squared distance from an axis of rotation (Meriam and Kraige, 1997). In our calculations, the axis of rotation was positioned anterior to the rostrum in a dorsoventral direction (i.e., running along the z-axis, Fig. 1C). The second moment of area, I, for both and streamlined bodies was calculated with the following equation:

$$I = \frac{\rho\pi}{4}\sum_{i=1}^{n}\left(\frac{1}{16}w^3h + why^2\right)_i \Delta y, \tag{4}$$

where Δy is the distance between transverse sections and y, h, and w are, respectively, the y-position, height, and width of the i^{th} section, for a total of n sections. Measurements of height and width were used to calculate the moment of inertia for the fish body, I_{fish} and Eq. 3 provided the dimensions to find the moment of inertia for the streamlined body, I_{NACA}. The streamlining index, S_L, was calculated as the ratio of these quantities:

$$S_L = \frac{I_{fish}}{I_{NACA}}. \tag{5}$$

The streamlining index was related to base-10 log-transformed values of body length with a logistic regression. This type of regression is appropriate for relating a proportion to a continuous variable (Sokal and Rohlf, 1995) and, in this case, was described by the following equation:

$$S_L(L) = \frac{e^{b_1 + b_2\mathrm{Log}_{10}L}}{1 + e^{b_1 + b_2\mathrm{Log}_{10}L}}, \tag{6}$$

which yields:

$$\ln\left(\frac{S_L}{1 - S_L}\right) = b_1 + b_2\,\mathrm{Log}_{10}L. \tag{7}$$

Values for the constants describing the intercept, b_1, and rate of change, b_2, were found by maximum-likelihood within Matlab (with the Statistics Toolbox 5.0).

Kinematics and Hydrodynamics

The posture of the fins during coasting was measured from video recordings of fish at different stages of growth. Coasting was recorded from a dorsal view with a high-speed, high-resolution video camera (500 frames s^{-1} at 1280 × 1024 pixels,

NAC Hi-Dcam II) focused on the center of the aquarium using a macro lens (50 mm Nikkor, Nikon) with a field of view ranging from ~4 to ~50 mm in width. We analyzed only those sequences where fish visibly maintained a constant posture to their fins, for a total of three coasting sequences per individual. Projected angles of fin posture from the dorsal view were measured with respect to the midline of the body for caudal, dorsal, and pectoral fins. The caudal fin angle was taken as half the angle between the dorsal and ventral lobes of the fin with respect to the peduncle. The dorsal fin angle was measured between the posterior fin base and lateralmost margin of the fin, with respect to its anterior margin. The pectoral fin angle was taken as the angle between the lateralmost point on the leading edge and the lateral surface of the body, with respect to the medial base of the fin. The fin angles for each coast were taken as the mean value from five video frames spanning the duration of the coasting phase.

The instantaneous positional changes in the body of coasting fish provided the basis for measurements of Reynolds number and in vivo drag coefficients. Changes in the position of fish were measured from video recordings of coasting (as in Osse and Drost, 1989) by autotracking a point between the eyes of fish using a custom Matlab program (methods detailed in McHenry and Lauder, 2005). The average Reynolds number, Re, was calculated using the mean speed, $\bar{U}$, of fish throughout a glide (Lamb, 1945):

$$Re = \frac{\rho \bar{U} L}{\mu}, \tag{8}$$

where ρ is water density, and μ is water viscosity. Consistent with the results of McHenry and Lauder (2005), fish were considered to operate in the inertial regime when $Re > 1{,}000$ and the viscous regime when $Re < 300$. The drag experienced by fish gliding in the intermediate regime ($300 < Re < 1{,}000$) was approximated as inertial drag and therefore treated the same way as fish at $Re > 1{,}000$.

The biomechanical simplicity of coasting allows in vivo measurements of drag coefficients. In the inertial regime, the drag on a coasting body may be found by calculating the inverse of instantaneous measurements of speed and then curve fitting the following equation to those measurements (Bilo and Nachtigall, 1980):

$$\frac{1}{U(t)} = jt + \frac{1}{U_o}. \tag{9}$$

We found the slope of this relationship, j, with a linear least-squares curve fit (in Matlab) and then used that value with the measured body mass, m, and wetted surface area, A_{body}, to calculate the inertial drag coefficient for a glide (modified from Bilo and Nachtigall, 1980):

$$C_{inert} = \frac{2j(m + \rho MV)}{\rho A_{body}}, \tag{10}$$

where M is the added mass coefficient (assumed equal to a 1:6 ellipsoid, $M = 0.045$; Munk, 1922; McHenry and Lauder, 2005) and V is the volume of the body, calculated from our volumetric reconstruction (see above). A similar approach was taken to find the viscous drag coefficient for fish operating at low Reynolds numbers. The following equation was curve-fit to measurements of body position using a nonlinear least-squares fit (McHenry and Lauder, 2005):

$$p(t) = U_o \tau (1 - e^{-t/\tau}), \tag{11}$$

where τ is the time constant. Values for the time constant found by curve-fitting were used to calculate the viscous drag coefficient from the following equation (McHenry and Lauder, 2005):

$$C_{visc} = \frac{m + M\rho V}{\tau L \mu}. \tag{12}$$

RESULTS

Locomotor Morphology

Our morphometric measurements tracked changes in body shape and the fins during growth. The bodies of larvae tapered posteriorly, with the greatest width at the eyes (Fig. 2A,B). The trunk and caudal regions became thicker over ontogeny, particularly in the growth from larval to juvenile stages (Fig. 2B,C), and thereby contributed to body streamlining. This trend continued in the growth between juvenile and adult stages (Fig. 2C,D), which was reflected in S_L measurements (Fig. 3A). S_L showed a rapid increase (from ~0.30 to ~0.75) in the growth from larval to juvenile stages and a smaller change (from ~0.75 to ~0.90) in subsequent growth. These changes were characterized by a logistic growth equation (Eq. 6), where $b_1 = -3.16$ and $b_2 = 3.69$ and L was given in millimeters.

Changes in the body shape of zebrafish were reflected by its allometric scaling. The exponential scale factor for body mass was slightly, but significantly, greater than isometry ($f = 3.17$; Fig. 3B, Table 1), which may be attributed to the allometric scaling of body volume ($f = 3.33$; Table 1). The largest few fish showed deviation above this trend in body mass that suggests a higher scale factor than the general trend for all stages (Fig. 3B). The allometric growth of the body was further reflected in the scaling of wetted surface area, which also exhibited small, but significant, deviations from isometry ($f = 2.16$; Fig. 3C, Table 1). Therefore, growth in body mass, volume, and surface area outpaced increases in body length as zebrafish adopted a streamlined form.

Positive allometric growth was found in the scaling of fin morphology. The distances spanned by the pectoral (Fig. 4A), dorsal and anal (Fig. 4C), and caudal (Fig. 4E) fins scaled by factors greater than predicted by isometry (Table 1). Although this suggests that adults have disproportionately larger fins than larvae, we found that the wetted surface area scaled with isometry in all but the pectoral fins (Fig. 4B,D,F). Therefore, the median fins changed their shape in a manner that increased their span while maintaining the same proportionate area.

Our measurements of fin posture during coasting demonstrated large behavioral variation that did not correlate with body size. Although we found fish of all sizes to maintain constant fin postures for the duration of the coasting phase, the angular orientation of the pectoral, dorsal, and caudal fins varied greatly between individuals of the same size and between coasts of the same individual (Fig. 5). For example, one juvenile ($L = 13.8$ mm) exhibited pectoral fin angles between 25.6° and 26.6°, while another ($L = 12.0$ mm) ranged between 30.7° and

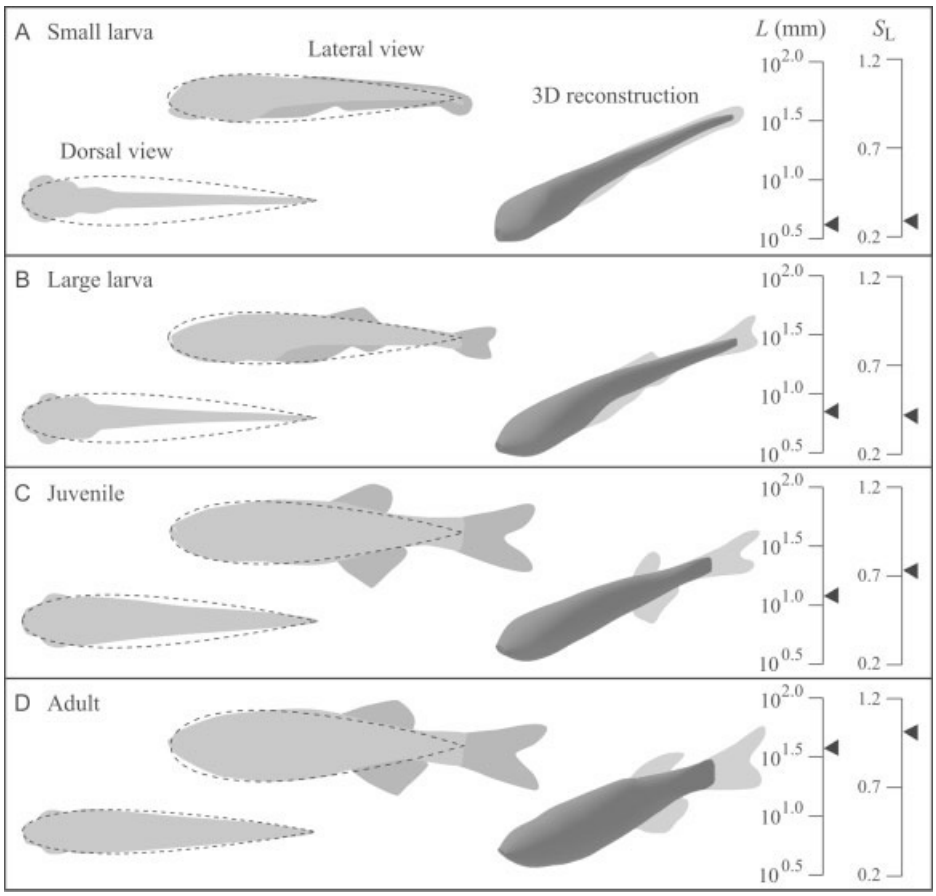

Fig. 2. The body shapes typical of zebrafish at different stages of growth. Representative individuals of **A:** small larvae, **B:** large larvae, **C:** juveniles, and **D:** adults are compared with the shape of a streamlined foil (dashed line). The gray silhouettes traced from digital photographs of dorsal and lateral views of the body were used to reconstruct its 3D shape (Fig. 1). The distribution of mass calculated from these volumetric data were compared to a streamlined body using the streamlining index, S_L (Eq. 5). Values for S_L are shown to the right with the body length, L, for each fish illustrated.

TABLE I. Scaling of morphology and hydrodynamics relative to body length in zebrafish

Dependent variable, y	Allometric relationship	f	f_{low}	f_{up}	f_o	α	r^2	n
Body mass, m	Positive	3.17	3.07	3.28	3	4.14×10^{-6}	0.99	23
Body volume, V	Positive	3.33	3.22	3.45	3	9.75×10^{-3}	0.99	23
Body surface area, A_{body}	Positive	2.16	2.11	2.22	2	3.06×10^{-1}	0.99	23
Body height, h_{max}	Positive	1.85	1.54	2.17	1	1.15×10^{-1}	0.86	23
Body width, w_{max}	Positive	1.56	1.26	1.85	1	6.22×10^{-2}	0.83	23
Pectoral fin span, s_{pec}	Positive	1.44	1.25	1.63	1	7.05×10^{-2}	0.97	12
Caudal fin span, s_{caud}	Positive	1.28	1.20	1.36	1	7.06×10^{-2}	0.98	23
Dorsal + anal fin span, s_{dors}	Positive	1.19	1.02	1.35	1	8.86×10^{-2}	0.90	23
Pectoral fin area, A_{pec}	Positive	2.84	2.49	3.18	2	2.00×10^{-3}	0.97	12
Caudal fin area, A_{caud}	Isometric	2.25	1.97	2.54	2	9.19×10^{-2}	0.92	23
Dorsal + anal fin area, A_{dors}	Isometric	2.08	1.74	2.42	2	1.62×10^{-1}	0.87	23
Reynolds number, Re	Isometric	2.26	1.98	2.54	2	1.53×10^{0}	0.93	23
Viscous drag coefficient, C_{visc}	Positive	1.74	1.48	1.99	0	5.24×10^{-2}	0.95	14
Inertial drag coefficient, C_{inert}	Negative	−2.34	0.87	3.82	0	1.44×10^{2}	0.60	9

The scale factor, f, and its lower, f_{low}, and upper, f_{up}, 95% confidence intervals, were compared with the isometric prediction, f_o, and are given with the scaling constant, α, and the coefficient of determination, r^2, for the reduced major axis regression of each dependent variable against body length ($y = \alpha L^f$).

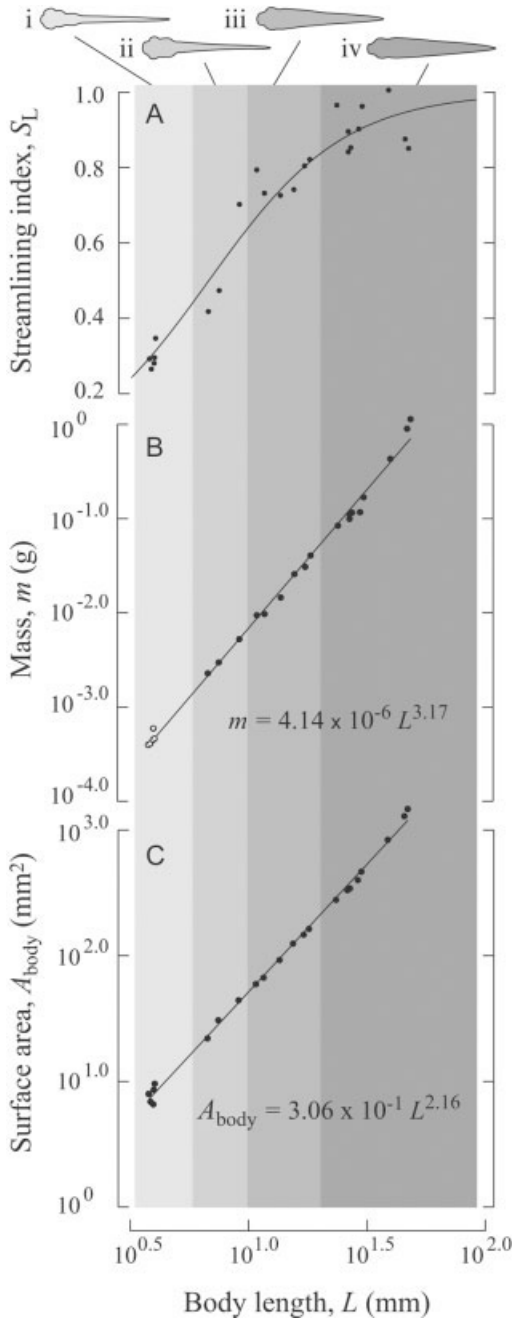

Fig. 3. The scaling of body morphology. Gray silhouettes show representative body shapes from a dorsal view of (i) small larva, (ii) large larva, (iii) juvenile, and (iv) adult stages and the corresponding columns denote the range of body lengths for each growth stage. **A:** The streamlining index is approximated by a logistic regression (Eq. 6) where $b_1 = -3.16$ and $b_2 = 3.69$. **B:** The scaling of body mass from direct (filled circles) and indirect (open circles) measurements from body volume data. **C:** The wetted surface area of the body was measured from its 3D reconstruction. See Table 1 for statistics.

66.8°. Furthermore, this behavioral variation did not correlate with growth stage (Fig. 5D). The standard deviation among the mean values of individuals (11.0°) was equal to the mean standard deviation within individuals and this variation had no relationship with body length, according to an ordinary least-squares regression ($P = 0.93$, $r^2 \ll 0.01$, n = 17). A similar lack of any correlation was found in angles for the dorsal ($P = 0.48$, $r^2 = 0.03$, n = 17) and caudal fins ($P = 0.50$, $r^2 < 0.01$, n = 17; Fig. 5B,C). The only apparent effect of size on fin posture was found in the dorsal fin angle (Fig. 5C), where values remained close to zero and exhibited little variation in individuals of $L < 13.5$ mm, but exceeded angles of 20°, at larger sizes. Observations of video recordings suggested that the smaller of these fish lacked the ability to abduct their dorsal fin.

Reynolds Number and Drag Coefficient

Measurements of Reynolds number and drag coefficient during coasting demonstrate changes in hydrodynamics due to growth in morphology and fin posture. Using the mean Reynolds number to identify hydrodynamic regimes, we found that adult fish ($L > 18.0$ mm) operated in either the inertial ($Re >$ 1,000) or intermediate ($300 < Re <$ 1,000) regimes and that larval and juvenile fish operated in the viscous regime ($Re < 300$; Fig. 6). Categorizing individuals into regimes allowed for the measurement of in vivo drag for fish of different size (Fig. 6B). We found that C_{visc} of larval and juvenile fish scaled by an exponential factor of 1.74 (Table 1) and C_{inert} decreased by a factor of −2.34 with body length in adult fish (Table 1).

DISCUSSION

How Does the Body Change Shape During Growth?

We found that zebrafish approach a streamlined shape at a variable rate over the course of development. Measurements of the streamlining index, S_L, showed logistic growth (Eq. 6, Fig. 3A) with a rapid increase in larvae and juveniles ($L < 18.0$ mm) and more gradual change in adults. This pattern suggests that zebrafish begin their life history around $S_L = 0.24$, which may be interpreted as a one-quarter similarity in volume distribution to a streamlined body. This increased to $S_L = 0.81$ by the beginning of the adult stage ($L = 18.0$ mm) and achieved values approximating a perfectly streamlined body ($S_L = 0.94$) in the largest adults ($L = 40$ mm).

Our introduction of S_L to fish morphometrics provides an improvement over linear measurements for providing a functional interpretation of body shape. For example, zebrafish larvae exhibit a posterior shift in body volume due to yolk absorption and dorsoventral growth in the trunk (Figs. 2, 3) that contributes to streamlining while maintaining a similar body depth. This change in

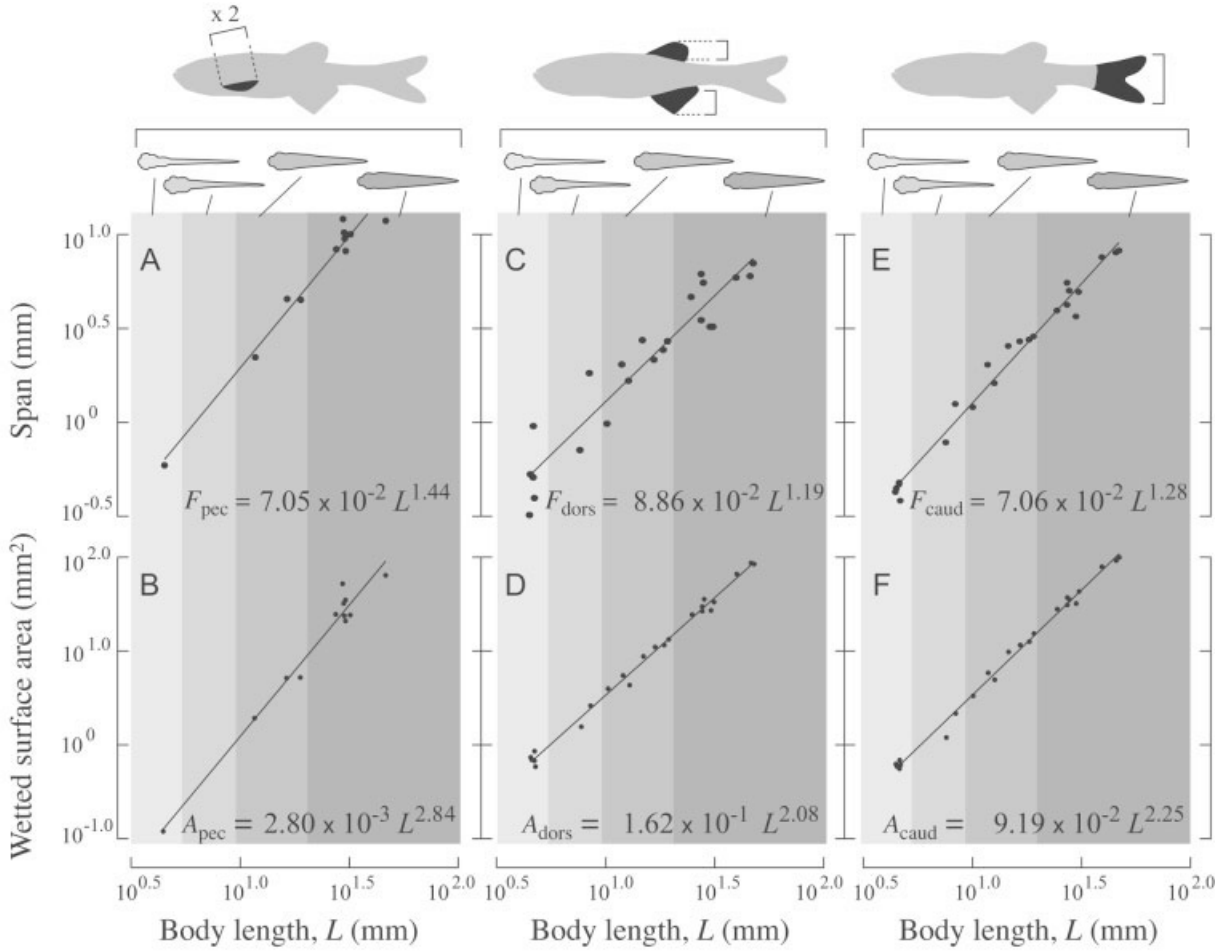

Fig. 4. The scaling of span and wetted surface area of the fins at rest. The location of pectoral (**A,B**), dorsal + anal (**C,D**), and caudal (**E,F**) fins are highlighted in black on gray silhouette drawings of the body (above) of an adult from a lateral view. Gray columns denote growth stages, as described in Figure 3. **A,B:** The span (**A**) and area (**B**) of the pectoral fins were measured from a perpendicular view of the fins. Values are equal to the sum for both fins. **C–F:** Measurements for the median fins were made from a lateral view. **C,D:** Values for the span of the dorsal and anal fins is equal to their sum and excludes the portion of the body between the fins. **E:** The span for the caudal fin is the distance between its dorsal and ventral margins. See Table 1 for statistics.

shape is reflected in measurements of S_L (Fig. 3A), but is neglected by simple linear measurement, such as the fineness ratio (body length divided by its maximum height).

The increase in body streamlining during growth affects other aspects of morphology that could influence locomotor mechanics. Adult zebrafish are relatively wide and tall compared to larvae, and therefore have disproportionately greater wetted surface area (Table 1, Fig. 3) that likely contributes to drag production (see discussion below). These changes in shape are also reflected in positive allometries in body volume and mass (Fig. 3B, Table 1). The large body mass of adult fish combines with their relatively high speed (McHenry and Lauder, 2005) to generate disproportionately greater momentum during the propulsive phase. This high momentum propels adult fish to travel proportionately further than larvae during coasting (McHenry and Lauder, 2005).

These results reflect prevailing patterns in the growth of zebrafish, but neglect some of the fine-scale changes in body shape that have been reported for other fish species. Some cyprinid fishes exhibit positive allometries in the width and height of the body (e.g., *Cyprinus carpio*; Hoda and Tsukahara, 1971) that are similar to what we report (Table 1). However, studies focused on the scaling of body shape with higher sampling have revealed subtle changes in allometric scaling between stages of growth (Hoda and Tsukahara, 1971; Fuiman, 1983; Webb and Weihs, 1986). Furthermore, zebrafish are sexually dimorphic as adults (Schilling, 2002), which implies sex-specific scaling in juvenile and adult fish. It would be interesting to examine the functional consequences of these fine-scale differences.

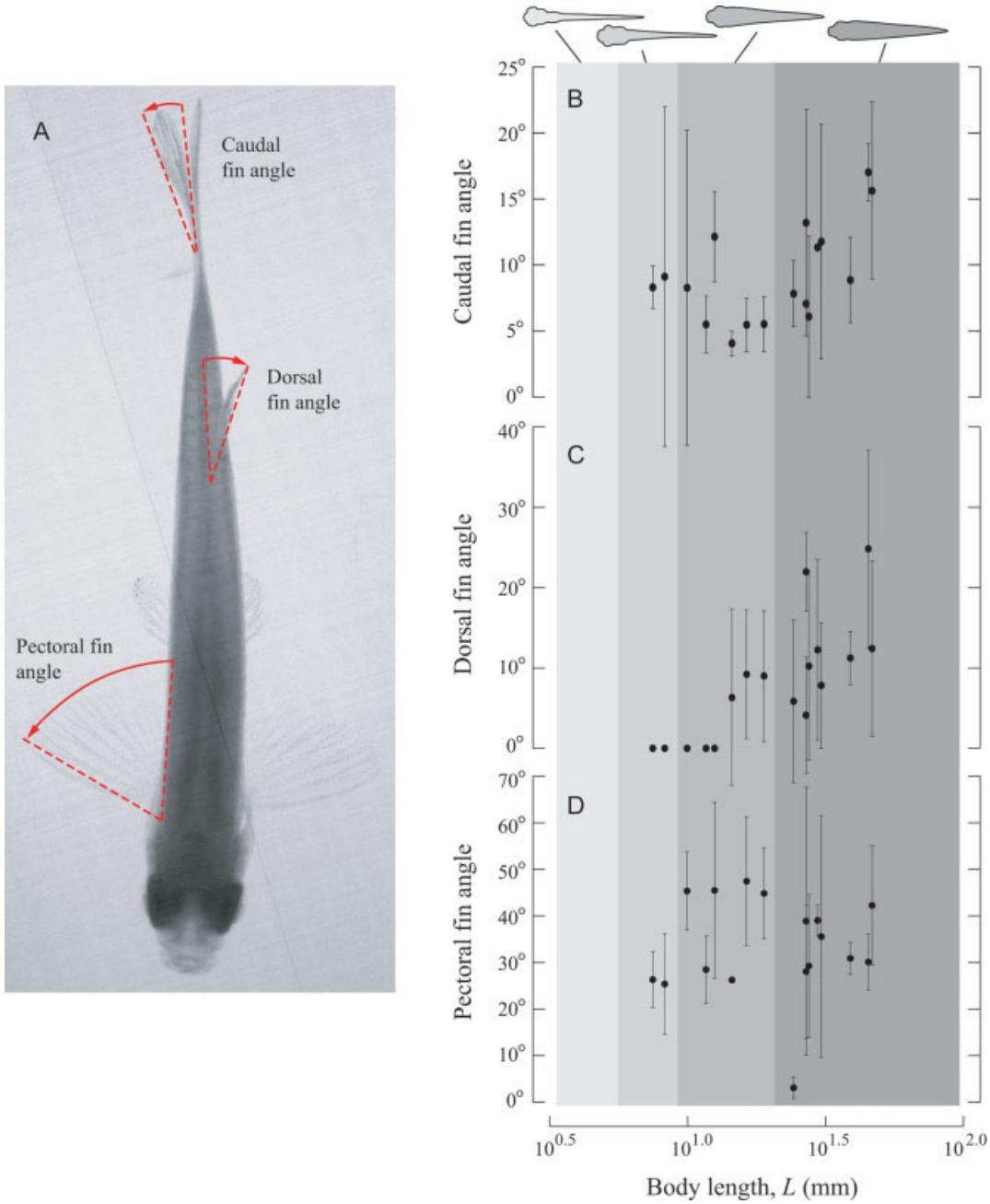

Fig. 5. Fin posture during coasting in fish of different size. **A:** Measurements of fin posture are illustrated on a video still from a coasting sequence of an adult. **B–D:** The mean (±1 SD) angle for three coasting sequences for each fish (n = 17) are plotted for the (**B**) caudal, (**C**) dorsal, and (**D**) pectoral fins against body length. Gray columns denote growth stages, as described in Figure 3. Data are absent for small larvae because fins were not visible on video recordings for that stage.

How Do the Size and Posture of the Fins Change During Growth?

Allometric changes in the fin morphology of zebrafish could influence the generation of locomotor forces and moments. Positive allometries in the span of fins (Table 1, Fig. 4) should enhance the generation of turning moments at later stages by providing disproportionately large moment arms and a heightened ability to generate thrust by vortex shedding (Dickinson, 1996; Drucker and Lauder, 1999). Such force generation may be further augmented by the disproportionately large area of the pectoral fins in adults (Table 1, Fig. 4A,B). The relatively high force required for turning moments in adults could be generated by their enlarged fin musculature (Thorsen and Hale, 2005). An increase in ability to generate turning moments is reflected in large shifts in direction during the propulsive phase of routine

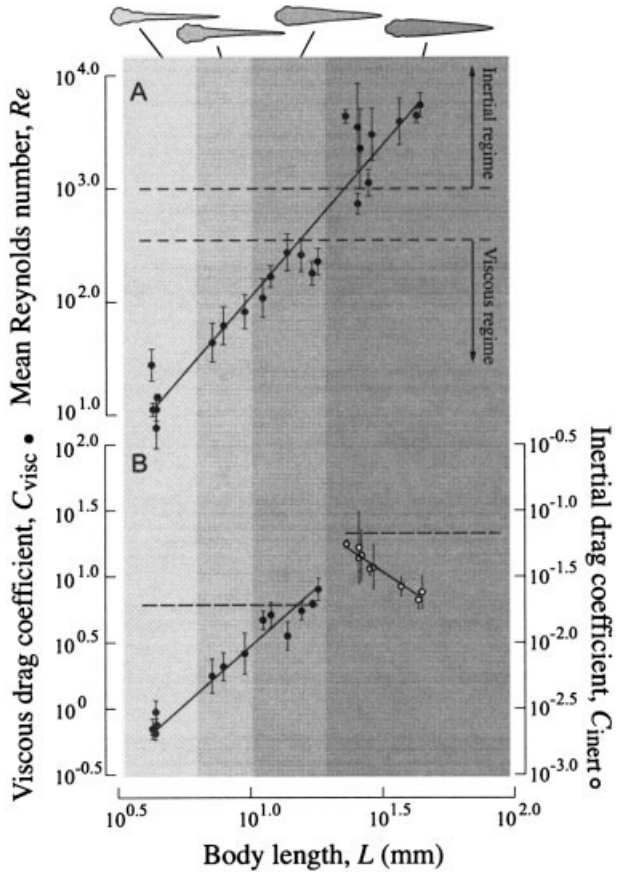

Fig. 6. The hydrodynamics of coasting in fish of different size. **A:** The mean Reynolds number (±1 SD) during coasting (n = 22, three sequences per individual) is shown in relation to hydrodynamic regimes (dashed lines) based on the "dead drag" measurements of McHenry and Lauder (2005). **B:** The in vivo viscous (filled circles) and inertial (open circles) drag coefficients (n = 22) are shown for the same coasting sequences. Dashed lines show the measured "dead drag" values for adults in the viscous and inertial regimes and gray columns denote growth stages, as described in Figure 3.

swimming in adults (Fuiman and Webb, 1988; McHenry and Lauder, 2005) and the small directional changes created by pectoral fin beating in larvae (Thorsen et al., 2005).

The amount of drag generated by a fin during coasting depends strongly on its posture. Fish are capable of rapid breaking by abducting and orienting their fins with a high angle of attack (Videler, 1981; Drucker and Lauder, 2001; Higham et al., 2005) that generates large drag force (Dickinson, 1996). We found that the angles of caudal and pectoral fins showed large behavioral variation that did not correlate with body size (Fig. 5B,D). This contrasts with the sigmoidal pattern of resting fin orientation reported by Thorsen and Hale (2005; their fig. 10) for the growth of the pectoral fins. Zebrafish apparently adjust the position of their pectoral fins during coasting so that no trend in posture is observed across ontogeny. Also, with development of contractile fin musculature in the juvenile stage, zebrafish acquire the ability to actively control drag forces and body stability by manipulating not only pectoral fin position, but also dorsal, anal, and caudal fin orientation. Locomotion may thus be behaviorally modulated in juvenile and adult fish by adjustment of all fin positions, not just the pectoral fins.

How Do Morphological Changes Affect Drag Coefficient?

Our measurements of drag coefficients evaluated the effects of ontogenetic change in body shape and fin posture on hydrodynamics. We found that the streamlined shape of large juvenile and tethered adult fish (McHenry and Lauder, 2005) possessed C_{visc} values that were about 10 times greater than small larvae (Table 1; Fig. 6B). This difference may be attributed solely to a disparity in shape because C_{visc} is a measure of viscous drag that normalizes for the effects of scale. It is for this reason that a zero scaling factor was predicted for the isometric scaling of C_{visc} within the viscous regime.

The low drag generated by larvae suggests that they have a body shape that is well suited to viscous hydrodynamics. In the viscous regime, drag may be reduced by minimizing the area exposed to the surrounding water. A spherical body provides the minimum wetted surface area for a given volume and thereby is predicted to generate relatively low drag. The elongated form of a larval body has a surface area that is much greater than a sphere, but is lower than an adult shape of the same volume (Fig. 3C). As larval zebrafish assume the shape of an adult and increase their proportionate wetted surface area, viscous drag increases (Table 1, Fig. 3C) and C_{visc} consequently scales with positive allometry (Fig. 6B).

Although viscous drag production increases in larvae and juveniles, the benefit of adopting a streamlined body becomes apparent in the adult stage. Adult fish routinely operate in the inertial regime (Fig. 6A), where a streamlined body shape provides a well-established optimum for reducing drag (Batchelor, 1967). As adults become more streamlined (Fig. 3A), the inertial drag coefficient decreases (Fig. 6B).

The rapid decline in the inertial drag coefficient with body length in adults suggests that small alterations in body shape have a marked effect on drag in the inertial regime. Although the rate of decline in adults is comparable to the rate of increase in larvae and juveniles (Table 1), the adult shape changes are more subtle (Fig. 3A). Therefore, change in body shape has a more pronounced effect on drag production in the inertial regime than in the viscous regime.

Growth of Form and Function in Aquatic Locomotion

Ontogenetic changes in behavior and morphology may have immediate functional consequences for aquatic locomotion. For example, the shell and mantle of the giant scallop (*Placopecten magellanicus*) grow in relative proportions such that thrust production is greatest relative to the submerged weight of the body in the middle of their life history, when they achieve their fastest swimming speeds (Dadswell and Weihs, 1990). Scyphozoan jellyfish (*Aurelia aurita*) decrease their pulse frequency as they become larger, which decreases their rate of thrust production and consequently their length-specific speed and energetic cost of transport (McHenry and Jed, 2003).

Instead of having an immediate impact on locomotor performance, some morphological or behavioral traits grow prior to their being able to play a functional role due to scale-dependent hydrodynamics. For example, some propulsive limbs grow in brine shrimp (*Artemia* sp.) before they are capable of generating thrust, but contribute to propulsion once the animal is large enough to operate with inertial hydrodynamics (Williams, 1994a,b). Therefore, the timing of a transition from viscous to inertial hydrodynamics influences whether growth has an immediate or delayed effect on the performance of aquatic locomotion.

Our results demonstrate how morphological growth has both immediate and delayed effects on the routine swimming of zebrafish. A zebrafish begins its life history with a body shape that generates relatively low drag in the viscous regime (Fig. 6B). The increase in C_{visc} during larval and juvenile growth illustrates immediate adverse consequences of growth on drag production when the fish operates in the viscous regime. The beneficial consequence of this change in body shape is delayed until the fish routinely operates in the inertial regime at the adult stage, when the streamlined shape of the body aids in reducing drag at high *Re*.

The timing of functional benefits and consequences to growth may differ between measures of performance or may vary with the behavior of the animal. For instance, zebrafish larvae are capable of reaching high, inertia-dominated *Re* values through their escape response (Fuiman and Webb, 1988; Budick and O'Malley, 2000; Muller and van Leeuwen, 2004). Unlike routine swimming, the performance of these rapid propulsive events should gradually increase over the entire course of growth as larvae become more streamlined. Therefore, the same pattern of growth that causes increased viscous drag production during routine coasting is likely beneficial to the performance of the inertial escape response.

Our results also inform evolutionary interpretations of growth in fish. Our finding that drag production rises during larval and juvenile growth contrasts with suggestions that ontogenetic changes in fish are well suited to the immediate functional demands of each stage of growth (Weihs, 1980; Webb and Weihs, 1986; Fuiman and Webb, 1988; Osse, 1990; Hale, 1996, 1999; Muller and Videler, 1996; Muller and van Leeuwen, 2004). We propose that low mechanical performance during a period of growth is an inevitable consequence of constraints on larval form or the differing functional demands of viscous and inertial regimes. Growth in morphology is unlikely to keep pace with the relatively rapid transition from viscous to inertial hydrodynamics. In zebrafish, change in shape largely precedes the hydrodynamic transition, but it is conceivable that such change could follow the transition in species large enough to operate in the inertial regime early in their life history. It would therefore be interesting to compare ontogenetic changes in the morphology and drag coefficients of related species of differing size to evaluate how heterochronic changes may relate to scale-dependent hydrodynamic performance.

ACKNOWLEDGMENTS

T. Griffin provided advice on mechanical scaling and F. Harrison, J. Strother, and an anonymous reviewer made numerous useful suggestions.

LITERATURE CITED

Batchelor GK. 1967. An introduction to fluid dynamics. New York: Cambridge University Press.

Bilo D, Nachtigall W. 1980. A simple method to determine drag coefficients in aquatic animals. J Exp Biol 87:357–359.

Budick SA, O'Malley DM. 2000. Locomotor repertoire of the larval zebrafish: Swimming, turning and prey capture. J Exp Biol 203:2565–2579.

Dadswell MJ, Weihs D. 1990. Size-related hydrodynamic characteristics of the giant scallop, *Placopecten magellanicus* (Bivalvia: Pectinidae). Can J Zool 68:778–785.

Dickinson MH. 1996. Unsteady mechanisms of force generation in aquatic and aerial locomotion. Am Zool 36:537–554.

Drucker EG, Lauder GV. 1999. Locomotor forces on a swimming fish: three-dimensional vortex wake dynamics quantified using digital particle image velocimetry. J Exp Biol 202:2393–2412.

Drucker EG, Lauder GV. 2001. Wake dynamics and locomotor function in fishes: interpreting evolutionary patterns in paired fin design. Am Zool 41:1431–1432.

Fuiman LA. 1982. Esocidae. In: Auer NA, editor. Identification of larval fishes of the Great Lakes Basin with emphasis on the Lake Michigan drainage. Ann Arbor: Great Lakes Fishery Commission.

Fuiman LA. 1983. Growth gradients in fish larvae. J Fish Biol 23:117–123.

Fuiman LA, Batty RS. 1997. What a drag it is getting cold: partitioning the physical and physiological effects of temperature on fish swimming. J Exp Biol 200:1745–1755.

Fuiman LA, Webb PW. 1988. Ontogeny of routine swimming activity and performance in zebra danios (*Teleostei: Cyprinidae*). Anim Behav 36:250–261.

Hale ME. 1996. The development of fast-start performance in fishes: Escape kinematics of the chinook salmon (Oncorhynchus tshawytscha). Am Zool 36:695–709.

Hale M. 1999. Locomotor mechanics during early life history: effects of size and ontogeny on fast-start performance of salmonid fishes. J Exp Biol 202:1465–1479.
Higham TE, Malas B, Jayne BC, Lauder GV. 2005. Behavior compensates for size: reducing pectroal fin area does not reduce breaking performance in bluegill sunfish (*Lepomis macrochirus*). J Exp Biol 208:4735–4746.
Hoda SMS, Tsukahara H. 1971. Studies on the development and relative growth of carp (*Cyprinus carpio*). J Fac Agric Kyushu Univ 16:387–509.
Hoerner SF. 1965. Fluid-dynamic drag. Brick Town, NJ: Hoerner Fluid Dynamics.
Huxley JS. 1932. Problems of relative growth. New York: Dial Press.
Ladson CL, Brooks CW, Hill AS, Sproles DW. 1996. Computer program to obtain ordinates for NACA airfoils. NASA Technical Memorandum 4741:1–22.
Lamb H. 1945. Hydrodynamics. New York: Dover.
McHenry MJ, Jed J. 2003. The ontogenetic scaling of hydrodynamics and swimming performance in jellyfish (*Aurelia aurita*). J Exp Biol 206:4125–4137.
McHenry MJ, Lauder GV. 2005. The mechanical scaling of coasting in zebrafish (*Danio rerio*). J Exp Biol 208:2289–2301.
McHenry MJ, Azizi E, Strother JA. 2003. The hydrodynamics of locomotion at intermediate Reynolds numbers: undulatory swimming in ascidian larvae (*Botrylloides* sp.). J Exp Biol 206: 327–343.
Meriam JL, Kraige LG. 1997. Dynamics. New York: John Wiley & Sons.
Muller UK, van Leeuwen JL. 2004. Swimming of larval zebrafish: ontogeny of body waves and implications for locomotory development. J Exp Biol 207:853–868.
Muller UK, Videler JJ. 1996. Inertia as a 'safe harbor': do fish larvae increase length growth to escape viscous drag? Rev Fish Biol 6:353–360.
Munk MM. 1922. Notes on aerodynamic forces. I. Rectilinear motion. NACA (Natl Adv Comm Aeronaut) TN No. 104:1–13.
Osse JWM. 1990. Form changes in fish larvae in relation to changing demands of function. Neth J Zool 40:362–385.
Osse JWM, Drost MR. 1989. Hydrodynamics and mechanics of fish larvae. Pol Arch Hydrobiol 36:455–466.
Osse JWM, van den Boogaart JGM. 2000. Body size and swimming types in carp larvae: effects of being small. Neth J Zool 50:233–244.
Rayner JMV. 1985. Linear relations in biomechanics — the statistics of scaling functions. J Zool 206:415–439.
Schilling TF. 2002. The morphology of larval and adult zebrafish. In: Nusslein-Volhard C, Dahm R, editors. Zebrafish. New York: Oxford University Press.
Sokal RR, Rohlf FJ. 1995. Biometry. New York: W.H. Freeman.
Thompson DW. 1917. On growth and form. Cambridge, UK: Cambridge University Press.
Thorsen DH, Hale ME. 2005. Development of zebrafish (*Danio rerio*) pectoral fin musculature. J Morphol 266:241–255.
Thorsen DH, Cassidy JJ, Hale ME. 2004. Swimming of larval zebrafish: fin-axis coordination and implications for function and neural control. J Exp Biol 207: 4175–4183.
Videler JJ. 1981. Swimming movements, body structure, and propulsion in cod (*Gadus morhua*). In: Day MH, editor. Vertebrate locomotion. Symp Zool Soc Lond p 1–27.
Webb PW, Weihs D. 1986. Functional locomotor morphology of early life-history stages of fishes. Trans Am Fish Soc 115:115–127.
Weihs D. 1980. Energetic significance of changes in swimming modes during growth of larval anchovy, *Engraulis mordax*. Fish Bull 77:597–604.
Westerfield M. 1995. The zebrafish book: a guide for the laboratory use of zebrafish, *Brachydanio rerio*. Eugene: University of Oregon Press.
Williams TA. 1994a. Locomotion in developing *Artemia* larvae: Mechanical analysis of antennal propulsors based on large-scale physical models. Biol Bull 187:156–163.
Williams TA. 1994b. A model of rowing propulsion and the ontogeny of locomotion in *Artemia* larvae. Biol Bull 187:164–173.